Low-Dimensional Maps Encoding Dynamics in Entorhinal Cortex and Hippocampus

Dmitri D. Pervouchine
dp@math.bu.edu
Department of Mathematics and Statistics and Center for BioDynamics,
Boston University, Boston, MA 02215, U.S.A.

Theoden I. Netoff
tnetoff@bu.edu
Department of Biomedical Engineering and Center for BioDynamics,
Boston University, Boston, MA 02215, U.S.A.

Horacio G. Rotstein
horacio@bu.edu
Department of Mathematics and Statistics and Center for BioDynamics,
Boston University, Boston, MA 02215, U.S.A.

John A. White
jwhite@bu.edu
Department of Biomedical Engineering and Center for BioDynamics,
Boston University, Boston, MA 02215, U.S.A.

Mark O. Cunningham
M.Cunningham@leeds.ac.uk
School of Neurology, Neurobiology and Psychiatry, University of Newcastle,
Newcastle upon Tyne, NE2 4HH, U.K.

Miles A. Whittington
M.A.Whittington@newcastle.ac.uk
School of Neurology, Neurobiology and Psychiatry, University of Newcastle,
Newcastle upon Tyne, NE2 4HH, U.K.

Nancy J. Kopell
nk@math.bu.edu
Department of Mathematics and Statistics and Center for BioDynamics,
Boston University, Boston, MA 02215, U.S.A.

Cells that produce intrinsic theta oscillations often contain the hyperpolarization-activated current I_h. In this article, we use models and dynamic clamp experiments to investigate the synchronization properties

of two such cells (stellate cells of the entorhinal cortex and O-LM cells of the hippocampus) in networks with fast-spiking (FS) interneurons. The model we use for stellate cells and O-LM cells is the same, but the stellate cells are excitatory and the O-LM cells are inhibitory, with inhibitory postsynaptic potential considerably longer than those from FS interneurons. We use spike time response curve methods (STRC), expanding that technique to three-cell networks and giving two different ways in which the analysis of the three-cell network reduces to that of a two-cell network. We show that adding FS cells to a network of stellate cells can desynchronize the stellate cells, while adding them to a network of O-LM cells can synchronize the O-LM cells. These synchronization and desynchronization properties critically depend on I_h. The analysis of the deterministic system allows us to understand some effects of noise on the phase relationships in the stellate networks. The dynamic clamp experiments use biophysical stellate cells and in silico FS cells, with connections that mimic excitation or inhibition, the latter with decay times associated with FS cells or O-LM cells. The results obtained in the dynamic clamp experiments are in a good agreement with the analytical framework.

1 Introduction

The hippocampus and entorhinal cortex (EC) are two major functional units of the medial temporal lobe memory system (Witter & Wouterlood, 2002). In these structures, the neural mechanism of memory is believed to be organized by the theta rhythm (4–12 Hz), which has been shown to exist in the EC and the CA1 region of the hippocampus in vivo and in vitro (Adey, Sunderland, & Dunlop, 1957; Adey, Dunlop, & Hendrix, 1960).

In both EC and the CA1, there is a cell type known to be able to autonomously produce oscillations in theta frequency range. In CA1, it is the oriens lacunosum-moleculare inhibitory interneurons (O-LM), shown to be critical for internal generation of the theta rhythm within area CA1 (Gilles et al., 2002). In medial entorhinal cortex (mEC) it is spiny stellate cells, also shown to possess robust theta-rhythmic properties (Dickson, Magistretti, Shalinsky, Hamam, & Alonso, 2000). However, the ability of individual cells to produce a theta rhythm does not imply the ability of a network to produce a coherent theta rhythm. Indeed, Rotstein et al. (2005) have shown through simulations that models of O-LM cells do not robustly synchronize unless there are other kinds of interneurons in the network, such as fast-spiking (FS) cells. The purpose of this article is to look more closely at the synchronization properties of networks that include these theta-producing cells in order to understand how the stellate cells and the O-LM cells interact with other cells in the superficial entorhinal cortex and hippocampus, respectively, to produce coherent theta and other rhythms.

Both of the cells described above have the hyperpolarization-activated current (h-current, I_h), thought to be important for the creation of the theta rhythm (White, Budde, & Kay, 1995; Dickson et al., 2000; Gillies et al., 2002). In these works, it has been shown that the interaction between I_h and other cation currents plays a critical role in subthreshold oscillations in stellate cells and in intrinsic membrane potential oscillations in O-LM cells. In this work, we explore how I_h interacts with inhibition to shape synchronization properties.

The effects of ionic currents on synchronization have been explored in other work (Crook, Ermentrout, & Bower, 1998; Ermentrout, Pascal, & Gutkin, 2001; Kopell, Ermentrout, Whittington, & Traub, 2000; Acker, Kopell, & White, 2003; Lewis, 2003). When the coupling is weak, this can be done with methods that average the effects of spikes over the cycle, but, as shown in Acker et al. (2003), this technique fails if the coupling is strong. One method that does not require weak coupling uses a spike-time-response curve (STRC), a function that measures the effects of a spike of a presynaptic cell on the timing of the next spike of the postsynaptic one. If there is no "memory" of the previous spike, STRCs can be used to construct spike time difference maps (STDM), which convey information about whether a pair of cell synchronizes (details are in section 2).

The STRCs and STDMs are a bridge between cellular biophysics and the behavior of a network in both in silico models and in vitro experiments. These techniques were used in Acker et al. (2003) and Netoff et al. (2004) to understand how the synchronization of a pair of stellate cells depends on key ionic currents important to the theta rhythm. In this article we expand that technique to networks involving more than one cell type and more than two neurons. We start with a network of two O-LM cells to provide a deeper understanding of the Rotstein et al. (2005) results and a foundation for and contrast to the work then presented on the larger networks: (1) a pair of stellate cells and a FS interneuron and (2) a pair of O-LM cells and an FS interneuron. The theoretical work on the EC network is supplemented by new experimental data produced using a dynamic clamp. These data both confirm the basic ideas of the model and present a puzzle that the theory is able to explain.

For the rest of the article, we refer to O-LM cells as O-cells, stellate cells as S-cells, and FS interneurons as I-cells. Here we consider three networks (see Figure 1). The first is mutual slow (20 ms decay time) GABA$_A$-mediated inhibition of a pair of O-LM cells (see Figure 1A). The next is a network with two S-cells connected with one I-cell with (5 ms decay time) GABA$_A$-mediated synapses from I-cell to S-cells and fast (3 ms decay time) AMPA-mediated synapse from S-cells to I-cell (see Figure 1B). The third is a network with two O-cells, each mutually coupled to an FS inhibitory cell with slow GABA$_A$-mediated synapses from the O-cell to the I-cell and fast GABA$_A$ synapse from the I-cell to the O-cell (see Figure C). In the second case, we show that the network can sometimes be reduced to that of a pair of
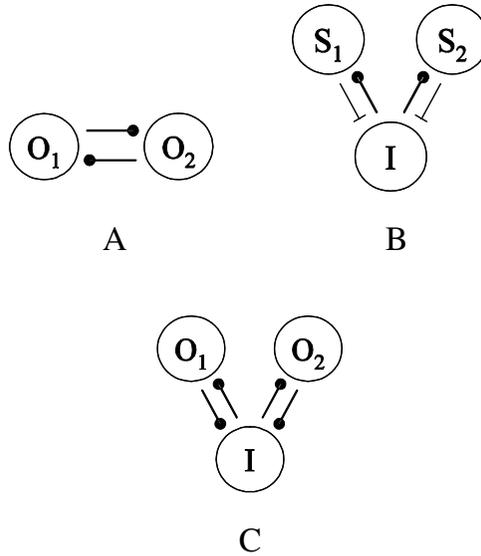
Figure 1: The networks: (A) O-O network with slow GABA$_A$-mediated synapses; (B) the S-I-S network with fast GABA$_A$ synapse from the I-cell to the S-cell and fast AMPA-mediated excitatory synapse from the S-cells to the I-cell; (C) the O-I-O network with slow GABA$_A$-mediated synapses from the O-cell to the I-cell and fast GABA$_A$ synapse from the I-cell to the O-cell.

stellate cells coupled by inhibition, perhaps also with an artificial inhibitory autapse on each stellate cell. However, aspects of the full three-cell system must be taken into account to understand the effects of noise, as occurs in the biological system. In the third case, the analysis of the three-cell system is a perturbation of the analysis of the network with one O-LM cell and one FS cell; the analysis shows why the I-cell synchronizes the two O-cells and shows the role of the long decay time of the inhibition produced by the O-LM cells.

2 Methods

2.1 Computational

2.1.1 Models of Neurons and Networks. The biophysical models of O-, S-, and I-cells use single-compartment representations of ionic currents that govern changes of membrane potential. They contain the standard components of the Hodgkin-Huxley model, fast Na$^+$, delayed-rectifier K$^+$, and leak currents. In addition, S-cells and O-cells contain the hyperpolarization-activated current (I_h), which consists of fast and slow components, and an

extra inward current active during the interspike interval. For the stellate cell, this is the persistent sodium current (I_{Nap}) as in previous models (Dickson, Magistretti, Shalinsky, Fransén, et al., 2000). For the O-LM cells we use the same formulation to model the extra inward current, although O-LM cells are not known to have the specific I_{Nap} current (Saraga, Wu, Zhang, & Skinner, 2003). An additional stationary current component I_{app} is chosen such that the neuron spikes periodically with a desired natural frequency. Values of the parameters are taken mainly from Acker et al. (2003) and Rotstein et al. (2005). The dynamic equations and parameters are summarized in the appendix.

It is known that both S- and O-neurons exhibit subthreshold oscillations that constrain the firing rate to 5 to 20 Hz over a large range of levels of depolarization (Lacaille, Williams, Kunkel, & Schwartzkroin, 1987; Maccaferri & McBain, 1996; Alonso & García-Austt, 1987; Dickson, Magistretti, Shalinsky, Hamam, et al., 2000). In most of the simulations, we chose the natural frequency of the S- and O-cells to be approximately 10 Hz. However, the results are robust to changes in these natural frequencies. The S-cells are connected to the I-cells using fast AMPA glutamatergic synapses; the I-cells are connected to S-cells using fast GABAergic inhibition (see Destexhe, Mainen, & Sejnowski, (1998) and Terman, Kopell, and Rose (1998) for models). Evidence for these connections comes from subthreshold responses of S- and I-cells to synaptic inputs (Jones & Buhl, 1993; Traub, Whittington, Colling, Buzsaki, & Jefferys, 1996; Cunningham, Daries, Buhl, Kopell, & Whittington, 2003), although it is not known whether excitatory postsynaptic potentials (EPSPs) onto the I-cells come from S-cells or pyramidal cells. The I-cells were connected to the O-cells using the same model as in Rotstein et al. (2005). The O-cells are connected to each other and to the I-cells using slow (but still GABA$_A$-mediated) GABAergic inhibition (Hájos & Mody, 1997). The synapse decay time (defined as the time it takes for the synaptic conductance to decrease to 37% of its maximum value) for the fast inhibition is taken to be approximately 5 ms, the measured value from the experimental data presented with this article. The synapse decay time for the slow inhibition is taken to be approximately 20 ms, the decay time measured for O-LM synapses onto pyramidal cells. The decay time of inhibitory postsynaptic potentials (IPSPs) from these cells onto interneurons has not been measured (however, see further discussion in Rotstein et al., 2005). Intermediate decay times of inhibition are also discussed.

2.1.2 Spike Time Response Method. The spike time response curve (STRC) measures how much a given perturbation changes the timing of a periodically spiking real or model cell (Acker et al., 2003). The input arrives a time Δ after the cell has spiked. We denote by $f(\Delta)$ the difference between the perturbed interspike interval and the natural interspike interval T (period of uncoupled cell); thus, $f(\Delta) > 0$ means the spike is delayed, and $f(\Delta) < 0$ means the spike is advanced. The graph of the function $f(\Delta)$ is
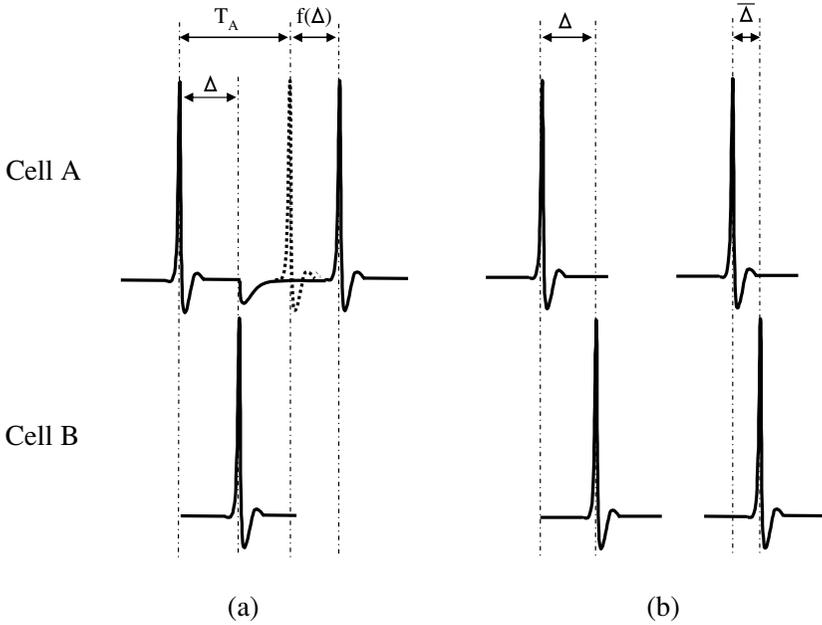
Figure 2: (a) Construction of spike time response curves. Δ is the time at which the inhibitory pulse arrives. T is the natural (unperturbed) interspike interval. $f(\Delta)$ is the difference between the interspike interval perturbed by the inhibitory pulse and T. (b) Spike time difference map is mapping that takes the difference in timing between the spikes of the two cells on one cycle (Δ) to the difference between those times on the next cycle ($\bar{\Delta}$).

the STRC (see Figure 2A). STRCs are essentially the same, up to a factor, as phase response curves (Ermentrout et al., 2001; Winfree, 1980); we find it more natural to work directly with time in a context of hybrid three-cell networks studied in this article. In what follows, we deal with several types of cells. Unless it is clear from the context, the corresponding STRC function will be denoted by $f_{AB}(\Delta)$, where A and B refer to the presynaptic cell and the postsynaptic cell, respectively.

We now consider a pair of cells that each fire periodically and are mutually coupled. Under some assumptions, discussed below, we can form a spike time difference map (STDM). The STDM takes the difference Δ in the spike times of the two cells in one cycle to that difference $\bar{\Delta}$ in the next cycle (see Figure 2B). We write the map as

$$\bar{\Delta} = \Delta + F_{AB}(\Delta). \tag{2.1}$$

The equilibrium state of equation 2.1, defined by

$$F_{AB}(\Delta) = 0, \tag{2.2}$$

is stable if

$$-2 < F'_{AB}(\Delta) < 0. \tag{2.3}$$

Otherwise, the equilibrium state is unstable (Strogatz, 1994). For more details about this method, see Acker et al. (2003).

Spike time response curves were obtained using custom software implemented in C++. Numerical integration was performed using standard adaptive step-size Runge-Kutta algorithm. The results of the simulations were visualized using Gnuplot's graphic interface and Matlab.

The STRCs and STDMs are influenced by all parameters in the system. The parameters that play the largest role in the analysis are g (the amplitude of the inhibitory conductance), g_h (the conductance of the h-current), I_{app} (applied DC current), and τ (the decay time of the inhibition). Unless we deal with one type of synapse, the synaptic amplitude is denoted by g_{XY}, where X and Y are the pre- and the postsynaptic neurons, respectively. In the simulations below, τ, g, and g_h are varied independently, while I_{app} is varied simultaneously with g_h to preserve the natural frequency (see the appendix).

2.2 Experimental. Methods in this article are similar to those used in Netoff et al. (2004). More detailed descriptions can be found in that article. All experimental results were obtained with entorhinal cortex stellate cells. The O-LM cells were assumed to be sufficiently similar in their intrinsic properties to stellate cells that STRC curves could be measured by inputs to stellate cells. The differences between the stellates and the O-LM cells in the networks are the kind of input that the cells receive. For example, the O-LM cells get input from other O-LM cells, which is inhibitory with a decay time of 20 ms. The stellate cells get only fast inhibition, with a decay time of 5 ms.

2.2.1 Electrophysiology. All experiments were conducted as approved by the Boston University Institutional Animal Care and Use Committee. Long-Evans rats 14 to 21 days old were anesthetized with isoflurane and decapitated. The brain was removed and chilled in ACSF (in mM, 126 NaCl, 1.25 NaH_2PO_4, 1.4-2 $MgSO_4$, 26 $NaHCO_3$, 10 Dextrose, 2 $CaCl_2$) and then sliced using a Vibratome to 350 μm thickness. Slices were bathed in a 34°C bath for 30 minutes and then let rest at room temperature for 30 minutes before experiments. Slices were then transferred to a heated (34–36°C) chamber (Warner Instruments, Hamden, CT), mounted on a fixed

microscope stage. Slices were perfused with heated ACSF aerated with 95% O_2 and 5% CO_2. Neurons within slices were visualized using differential interference contrast video microscopy (Zeiss AxoSkop FS2+, Dage/MTI CCD camera). Whole cell patch clamp recordings were obtained using patch pipettes (4–6 MΩ) fabricated from borosilicate glass (1.0 O.D. 0.75 I.D., Sutter Instruments, Novato, CA) and filled with (in mM), 120 K-gluconate, 10 KCl, 10 HEPES, 4 Mg-ATP, 0.3 Tris-GTP, $10Na_2$ − phospocreatine, and 20 creatine kinase and brought to pH 7.25 with KOH.

Recordings of stellate cells were made from the cell-dense layer 2. Stellate cells were identified electrophysiologically under current clamp, based on the presence of slow, inward-rectifying cation current (I_h) and brief first-spike latency (Alonso & Klink, 1993). All neurons included in this study were identified as S-cells. All the experiments were done without any pharmacological blockers of background activity. In previous work on the construction of STRCs in stellate cells, such blockers were found not to change the qualitative behavior of the results (Netoff et al., 2004).

2.2.2 Dynamic Clamp and Spike Time Response Curves. A real-time experimental control system (Dorval, Christini, & White, 2001) was used for a number of manipulations in these experiments, including controlling spike rate, delivering artificial synaptic conductance inputs, and building hybrid neuronal networks. The system is built on top of a real-time version of the Linux operating system. It is publicly available and can be downloaded from our web site (http://bme.bu.edu/ndl). The dynamic clamp was run at 10 kHz with a jitter on the order of 10–15 μs and response latency of one time step.

Spike time response curves were generated by delivering artificial inhibitory conductance inputs (IPSGs) to periodically firing neurons and measuring induced changes in spike timing. Artificial synaptic inputs were delivered only once per six firing cycles to minimize interactions of the synaptic inputs to allow us to track and control the baseline firing rate (see below) and confirm that the effects of artificial synaptic inputs lasted only one cycle (Netoff et al., 2004). The phase of the synaptic input was chosen using a pseudo-random Sobol sequence (Press, Teukolsky, William, & Brian, 1992) to sample the phase interval optimally with a finite number of choices.

The synaptic conductance waveform used followed the form $g_{syn} = g_s(e^{-t/\tau_r} - e^{-t/\tau})/k$, where g_s is the maximal synaptic conductance, t is the time since the initiation of the synaptic event, τ_r is the synaptic rise time constant, τ is the synaptic decay time constant, and k is a normalization factor. Synaptic time constants used were measured directly from spontaneous synaptic events in the S-cells as previously reported (Netoff et al., 2004). We found $\tau_r = 2.5$ ms and $\tau = 5$ ms for IPSGs. The current injected is calculated in real-time $I_s = g_{syn}(V_m - V_s)$, where V_m is membrane potential and

V_s is the synaptic reversal potential. This signal was scaled appropriately, converted to an analog signal, and passed to the current-drive channel of the bridge-balance amplifier (Axon Instruments 700B, Union City, CA). The measured value of V_m was updated, and a new value of I_s calculated and delivered, at a clock rate of 10 kHz. For EPSGs, $\tau_r = 1.68$ ms and $\tau = 6.21$ ms were used. The reversal potentials of excitatory and inhibitory synapses were 0 mV and -70 mV, respectively.

The experiments measuring STRCs were done at a control period of 100 ms, while the ones concerning antiphase (see Figure 8) used a baseline period for an uncoupled cell at about 137 ms. The latter were done first and showed the antiphase, as expected. However, it was difficult to get the uncoupled stellate cells to fire periodically at that slow rate, and so the STRC experiments were done at a higher control frequency.

The h-current was altered by blocking with ZD7288 and by adding that current artificially with the dynamic clamp. Unfortunately, the blocking experiment was not technically possible because ZD7288 depolarizes the cell, which can then compensate using the dynamic clamp's spike rate controller. However, the neurons consistently went into depolarization block after 1 or 2 minutes, preventing a good estimation of the STRC using our technique. Addition of extra h-current was done as in Dorval et al. (2001).

Spike time response curves were determined from responses to hundreds of artificial synaptic perturbations. Both the x-values (time of synaptic input minus time of last postsynaptic action potential) and y-values (change in timing of next action potential, relative to the unperturbed value) were typically normalized by the average unperturbed interspike interval. The average values of STRC were fit as explained in curve fitting section of the appendix.

3 Results

3.1 O-O Network. In this section we consider a network that consists of two mutually coupled O-cells (see Figure 1A). The STRC relevant for this network is $f_{OO}(\Delta)$, for which $\tau = 20$ (see Figure 3A for dependence of these curves on g_h; Figure 3B shows the experimentally determined STRC for one value of g_h). As shown, the numerical STRCs are qualitatively similar to experimental STRCs (see section 4 for details).

Suppose O_1 spikes at time t_1, and O_2 spikes at time $t_2 > t_1$. Denote $t_2 - t_1$ by Δ. The spike of O_2 makes O_1 spike at time $\bar{t}_1 = t_1 + T + f_{OO}(\Delta)$, where T is the period of the O-cell. The second spike of O_1 makes O_2 spike at time $\bar{t}_2 = t_2 + T + f_{OO}(\bar{t}_1 - t_2)$. Therefore, $\bar{\Delta} = \bar{t}_2 - \bar{t}_1 = t_2 + T + f_{OO}(T + f_{OO}(\Delta) - \Delta) - (t_1 + T + f_{OO}(\Delta)) = f_{OO}(T + f_{OO}(\Delta) - \Delta) - f_{OO}(\Delta) + \Delta$.

Here we assume that neither cell spikes twice in the absence of firing of the other, so the cells alternate their action potentials. The necessary
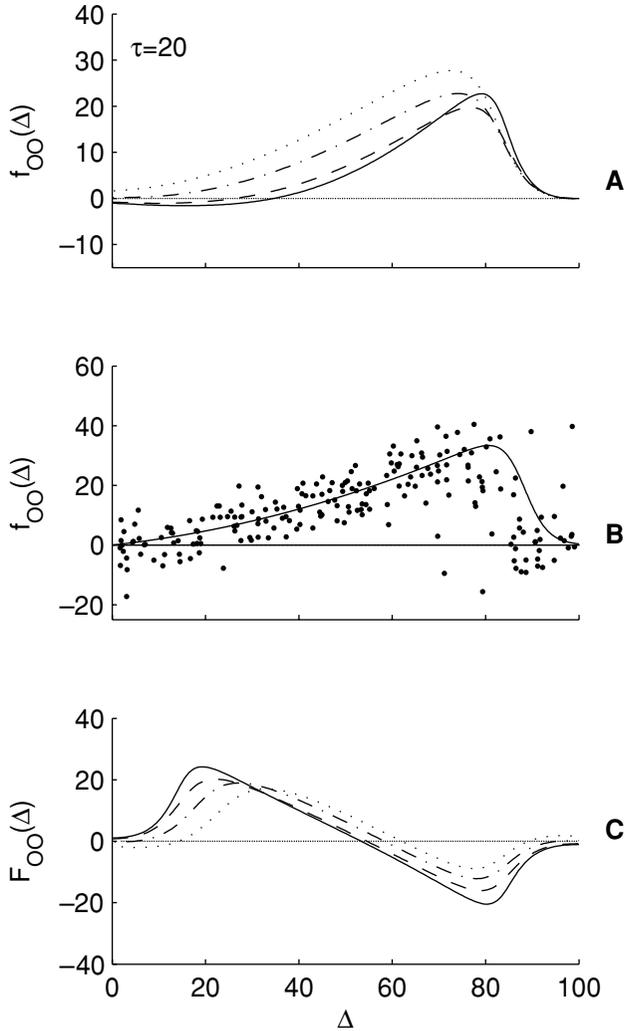
Figure 3: A family of slow inhibitory STRCs ($\tau = 20$ ms, $g_{OO} = 0.20$) depending on the conductance of the h-current (g_h). (A) STRCs computed from the model. The values of g_h are 1.5, 1.0, 0.5, and 0.3 (solid, dashed, dot-dashed, and dotted, respectively). The conductance of the h-current and the bias DC current are varied simultaneously to maintain the neuron's natural spiking period at ~ 100 ms. The corresponding compensatory values of I_{app} are -2.007, -0.879, 0.257, and 0.695. The reversal potential is -70 mV. (B) STRCs measured in the dynamic clamp experiment, $g_{OO} = 5$ nS (dots). (C) Spike time difference maps for the O-O network. Line types are the same as in *A*.

conditions for this are $\bar{t}_1 > t_2$ and $\bar{t}_1 < t_2 + T$. That is, $T + f_{OO}(\Delta) - \Delta > 0$ and $f_{OO}(\Delta) - \Delta < 0$. Equivalently,

$$\Delta - T < f_{OO}(\Delta) < \Delta. \tag{3.1}$$

Condition 3.1 is met for all STRCs in Figure 3A. Then for the spike time difference map, we have

$$\bar{\Delta} = \psi_{OO}(\psi_{OO}(\Delta)) = \Delta + F_{OO}(\Delta), \tag{3.2}$$

where

$$\psi_{OO}(\Delta) = T + f_{OO}(\Delta) - \Delta. \tag{3.3}$$

The function $\psi_{OO}(\Delta)$ is interpreted as follows. While $f_{OO}(\Delta)$ measures the spike time change (positive or negative) caused by the stimulus that arrives at time Δ after the previous spike, the function $\psi_{OO}(\Delta)$ measures the difference between the time of the stimulus and the time of the next spike. In the O-O network, where cells are mutually coupled, the time difference between the stimulus and the next spike for the first cell is equal to the time difference between the previous spike and the stimulus for the second cell. This leads to the second power of ψ_{OO} in equation 3.2.

These STRCs were used to construct the STDMs according to equations 3.2 and 3.3. The STDMs for the four different values of are plotted in Figure 3C. The STDMs have x-intercepts at 50 to 60 ms, with the slope between -2 and 0. These intercepts are referred to as *antiphase* equilibrium points.

In all situations shown above, with g_h not equal to zero, the antiphase solution is stable according to equation 2.3. Changes in strength of the synaptic coupling do not change the stability of the antiphase solution (data not shown). A decrease in g_h causes the position of the x-intercept to increase; that is, the interspike interval of the coupled O-cells is effectively shortened compared to the uncoupled cells.

There is also an in-phase solution, corresponding to $\Delta = 0$. Figure 3C shows that this point is unstable when $g_h = 1.5$, our baseline value, but becomes stable as g_h decreases; note that the slope of F at $\Delta = 0$ changes from positive to negative. That the decrease in the h-current, with $\tau = 20$, facilitates the stability of the synchronous solution was confirmed by numerical simulations (Rotstein et al., 2005).

3.2 S-I-S Network

3.2.1 Reduction to 2-Cell Network.   This network (see Figure 1B) contains three cells, so it is not immediately clear from the previous work how to use STDM methods to examine the stability of any solutions. We first show that under some hypotheses, the analysis of this network can be reduced to that of a related two-cell network. The hypotheses are:

1. The I-cell does not fire in the absence of phasic inputs from the S-cells.

2. An EPSP from either of the S-cells is sufficient to make the I-cell fire.

3. The firing pattern has the I-cell spike between the spikes of the S-cells, which alternate in firing (i.e., $S_1 - I - S_2 - I - S_1 - I \ldots$);

4. The effect of the I-cell inhibition on the S-cell that causes the I-cell to spike is small (because of the timing of the inhibition on that cell) and can be ignored without changing the qualitative results.

5. The delay between the firing of an S-cell and the firing of the I-cell that it induces is minimal and can be ignored.

Hypothesis 4 is the central one in the reduction to a two-cell model. By removing the effect of an I-cell on the S-cell that caused the I-cell to spike, the effect of an S-cell spike becomes a (slightly) delayed inhibition on the second S-cell. Therefore, at least when the two S-cells do not spike very close in time, the network is a pair of S-cells connected by inhibition. This is very similar to that of the O-O network analyzed in the previous section, but with a smaller decay time of the inhibition ($\tau = 5$ is the value measured for IPSPs onto the stellate cells). After the analysis of this two-cell network, we will revisit hypotheses 4 and 5.

The STRC relevant to this situation is f_{IS}, in which the S-cell gets inhibition with a decay time of $\tau = 5$ ms. Figure 4A shows numerical simulations of these STRCs with several levels of g_h. The major effect of the h-current is to advance the spike of the S-cell; the larger the g_h, the larger this effect. Parts B_1 and B_2 of Figure 4 show the experimentally determined STRCs, with inhibitory pulses fed to a real S-cell via dynamic clamp (see methods); Figure $4B_2$ is done with extra I_h current added with the dynamic clamp. As shown, the numerical and experimental STRCs behave in similar ways as g_h is changed: adding extra g_h causes the advance portion of the STRC in the beginning of the period (i.e., where $f(\Delta) < 0$) to increase. The experimental STRCs are consistent across cells, as Figure 5 shows.

The STDM that embodies the above hypotheses can help us understand if there is an antiphase solution and if it is stable; this STDM cannot say anything about the stability of solutions in which the S-cells are synchronous, since that solution violates the above hypotheses; synchrony needs to be looked at separately. The derivation of the STDM is exactly the same as that of the previous section, this time using the STRC corresponding to $\tau = 5$.
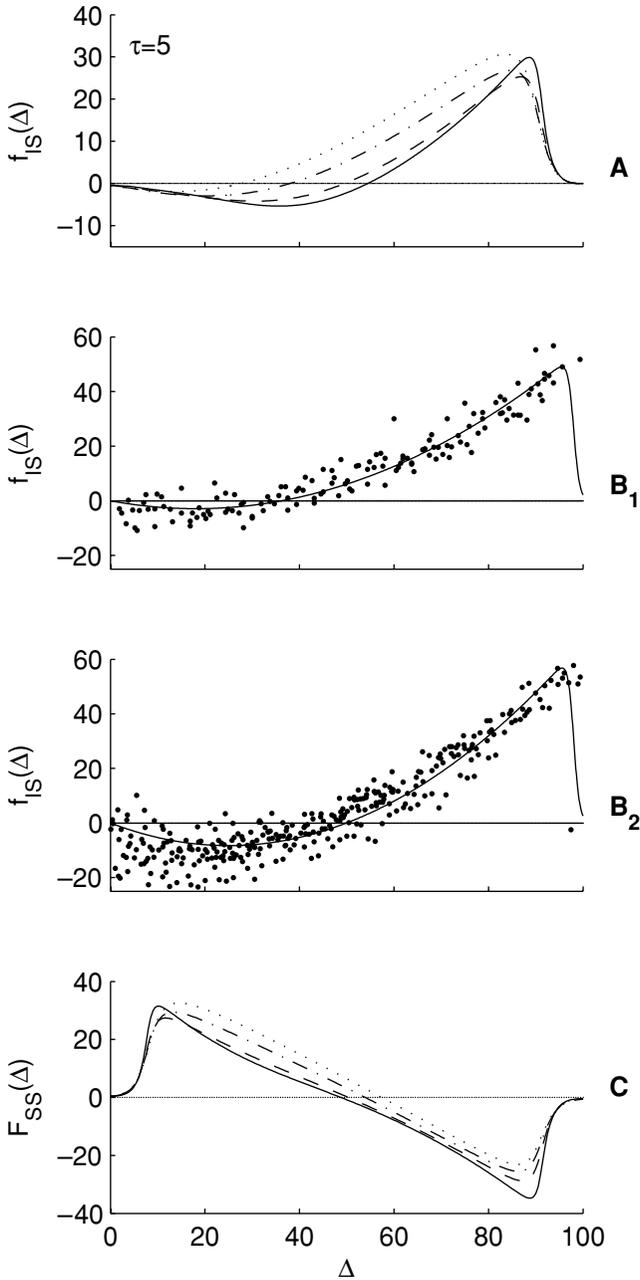
Figure 4: A family of fast inhibitory STRCs ($\tau = 5$ ms, $g_{IS} = 0.20$) depending on g_h. The rest of the legend is the same as in Figure 3 ($g_h = 15$ nS). Panel B_2 has an additional 10 nS of g_h applied compared to B_1.
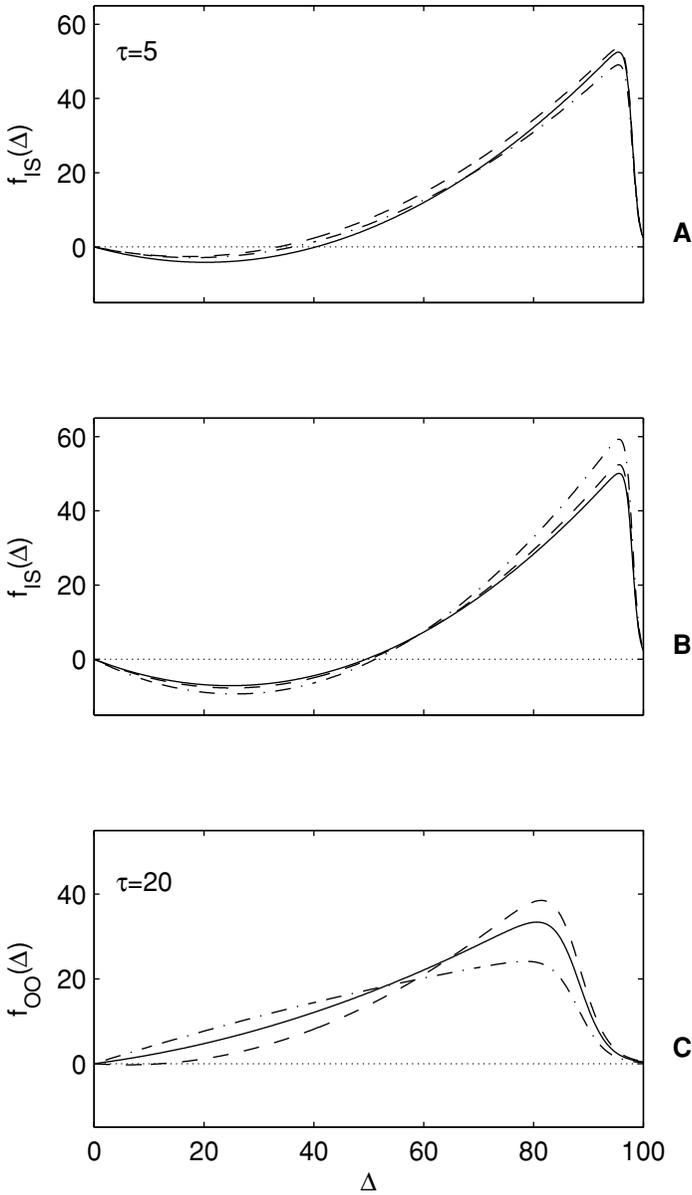
Figure 5: Variation of STRCs across cells. Fast inhibitory STRCs ($\tau = 5$ ms) for three cells are shown for basal level of g_h (A), and for increased level of g_h (B; additional 10 nS of g_h applied). Slow inhibitory STRCs ($\tau = 20$ ms) (C).

For later work, we will need these equations explicitly, so we write the STDMs as

$$\bar{\Delta} = \psi_{IS}(\psi_{IS}(\Delta)) = \Delta + F_{SS}(\Delta), \tag{3.4}$$

where

$$\psi_{IS}(\Delta) = T + f_{IS}(\Delta + \delta) - \Delta. \tag{3.5}$$

T is the natural spiking period of the S-cell, and δ is the time lag between firing of an S-cell and the firing of the I-cell that it induces (see hypothesis 5). The domain of validity of equation 3.4 is given by

$$\Delta - T < f_{IS}(\Delta + \delta) < \Delta. \tag{3.6}$$

Now assume that the value of δ is equal to 0. Then condition 3.6 is met for all STRCs in Figure 4A. The STDMs for the S-I-S network is given in Figure 4C. Note that the antiphase solution is stable for all values of the conductance of the h-current shown in the figure. As in the O-O case, the stability and position of the antiphase equilibrium points do not change with changing the strength of the inhibitory synaptic coupling (data not shown). A decrease in g_h causes the equilibrium phase to increase. This observation correlates with the dynamic clamp experiments, where adding extra h-current component noticeably shortened the interspike interval in the S-I-S network (data not shown).

3.2.2 Embedding 2-Cell Network Back in the 3-Cell Network. We now revisit assumption 4 and show that it does not make a qualitative difference in the behavior of the network. We replace the connection from the I-cell to the S-cell (e.g., S_1) that caused it to spike, but (for now) keep the delay from the S-cell spike to the I-cell spike at zero. We assume that there is a small time delay in the onset of inhibition in the S-cell, corresponding to the buildup of inhibition.

The inhibition on S_1 creates a kind of self-inhibition that delays the next spike of the S-cell. However, it does not introduce another degree of freedom, since that inhibition occurs with a time course fixed with respect to the time of the S-cell spike. Thus, the S-I-S network can still be treated as a two-cell network, but with an inhibitory "autapse" on the S-cell.

To see quantitatively the effect of this addition, we compare the usual STRC of inhibition onto an S-cell, with one computed by adding (artificial) self-inhibition onto the S-cell. Since the self-inhibition changes the "natural" period of the S-cell, we change the timescale of the latter to be the same as the S-cell without self-inhibition. Figure 6 shows that
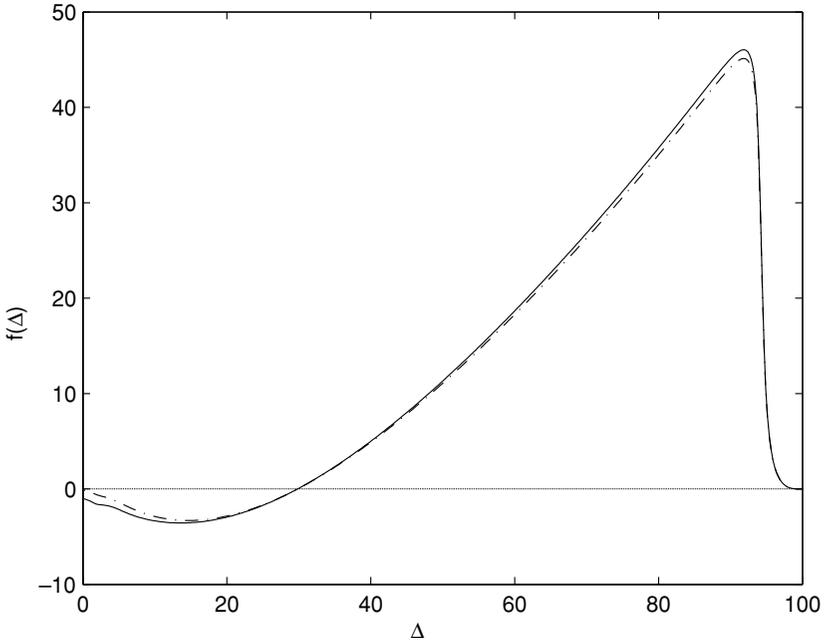
Figure 6: Fast inhibitory STRCs computed with adding self-inhibition onto the S-cell (dashed-dotted) and without it (solid). The time axis was scaled to 100 ms in both cases. The natural periods of the S-cell with and without self-inhibition were 100.0 and 102.6 ms, respectively.

the difference between them is tiny. Thus, the essential effect of the self-inhibition is a scaling of the STRC, which does not change qualitative behavior.

However, such scaling has an important consequence for the entire S-I-S network: if we compare an isolated stellate cell with an S-cell in the network, the period of the S-cell changes much less for the coupled cell when I_{app} is varied (data not shown).

3.2.3 Infinitesimal Delays. An excitatory synapse to some kinds of neurons (type 1) can cause a spike in the postsynaptic cell after some delay. The delay can be very sensitively depending on initial conditions and the size of the EPSP. In the previous sections, we assumed that the delay from the time the I-cell received excitation to the time it fired was zero (assumption 5). We now revisit that hypothesis, assuming that S-to-I synapses are strong; in this case, the delay is nonzero but very small and the same from cycle to cycle.

First, we estimate analytically how the antiphase solution changes when δ is varied infinitesimally. Let Δ_δ be the value of Δ for the antiphase solution when the delay is δ. It is a fixed point not only of F_{SS} but also of ψ_{IS}, that is,

$$T + f_{IS}(\Delta_\delta + \delta) - \Delta_\delta = \Delta_\delta. \tag{3.7}$$

From equation 3.7, $f_{IS}(\Delta_0) = 2\Delta_0 - T$. Using the first-order Taylor expansion of $f_{IS}(\Delta_\delta + \delta)$ at $\Delta = \Delta_0$ and expressing Δ_δ from the linear equation obtained, we get

$$2\Delta_\delta = 2\Delta_0 + f'_{IS}(\Delta_0)(\Delta_\delta + \delta - \Delta_0),$$

and therefore

$$\Delta_\delta = \Delta_0 + \frac{f'_{IS}(\Delta_0)}{2 - f'_{IS}(\Delta_0)}\delta. \tag{3.8}$$

Thus, the change in Δ_δ per 1 ms of delay is $f'_{IS}(\Delta_0)/(2 - f'_{IS}(\Delta_0))$; it is close to zero when $f'_{IS}(\Delta_0)$ is small and increases as $f'_{IS}(\Delta_0)$ gets close to 2. Note that in Figure 4C, Δ_0 is close to the middle point of the period, where $f'_{IS}(\Delta_0)$ ranges from 0.5 to 1. Thus, we predict that the change in Δ_δ is the same order of magnitude as δ, or may be even smaller depending on $f'_{IS}(\Delta_0)$.

We now go back to equation 3.4 and compute $F_{SS}(\Delta)$ numerically using $\psi_{IS}(\Delta)$ from equation 3.5. Note that the function $\psi_{IS}(\Delta)$ is defined for $\Delta \in [\delta, T - \delta]$. The function $F_{SS}(\Delta)$ is shown in Figure 7 for several values of δ. Note that the change in Δ_δ is smaller than δ, as predicted by equation 3.8, and the antiphase solution remains stable as δ increases up to 15 ms.

Thus, when S-to-I synapses are strong, the stability of the antiphase solution does not change even with delays as long as 15 ms. However, weak S-to-I synapses lead to a different result, as we show in the next section.

3.2.4 Large Delays and Noise. We now explain an otherwise puzzling observation about the S-I-S experimental data. The first set of experiments done with the three-cell network and the dynamic clamp technology used weak synaptic connections from the S-cells to the in silico I-cells. In this situation, the results did not replicate the predicted antiphase behavior between the S-cells. Instead, the phase lags appeared almost random, clustering about both antiphase and in-phase fixed points. When a larger value of the S-I synaptic conductance was taken, the predicted antiphase was found (see Figure 8). These experiments were done with a control period of approximately 140 ms instead of the 100 ms used in the experiments described above.
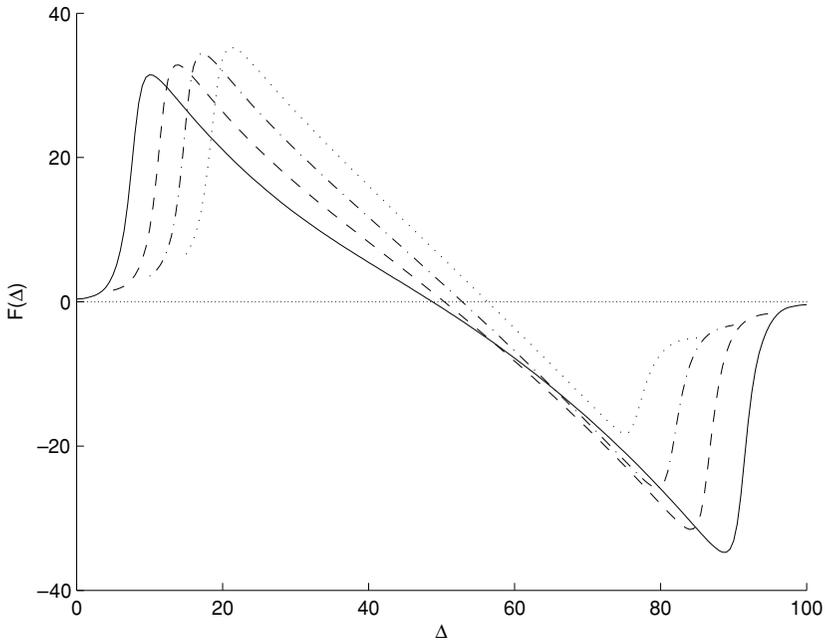
Figure 7: Spike time difference maps for the S-I-S network with delays: $\delta = 0$ ms (solid), 5 ms (dashed), 10 ms (dot-dashed), and 15 ms (dotted); $g_{IS} = 0.04$, $g_{SI} = 0.10$.

To understand the origin of this phenomenon, we look at the sources of variation in our system. There are two independent such sources. One is the delayed response of the I-cell to weak phasic EPSPs coming from the S-cells. The other is the noise that arises from ionic currents in the S-cells (e.g., persistent Na$^+$ current) and leads to spread of their firing times.

We next ask whether each of these sources alone can account for the difference in distribution of phases between S-cells in the dynamic clamp experiment. Figure 9 shows simulation of the full three cell network at the following conditions: with weak versus strong S-to-I synapses and high versus low levels of noise. The noise in S-cells, which was modeled by stochastic persistent Na$^+$ channels (see the appendix), leads to an even distribution of phases only if S-to-I synapses are sufficiently weak, that is, if the delay δ is sufficiently large. Thus, one needs both a high level of noise and large delays in order to get such distribution of phases (compare to Figure 8).

The critical question here is how the system escapes from the antiphase fixed point, which is stable in the deterministic case even if δ is large (see
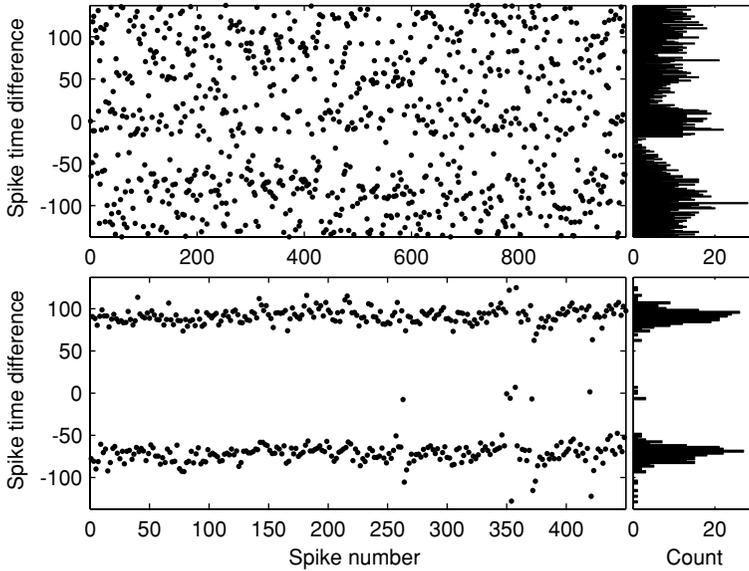
Figure 8: Evolution of spike time differences between two patch-clamped S-cells coupled through an I-cell with artificial synapses. The period of the un-coupled cells is 137 ms. Upper panel (weak synapses): The excitatory synapses are $g_{SI} = 10$ nS. The inhibitory synapses are $g_{IS} = 3$ nS. The average lag from EPSG to firing of I-cell is 16 ms. Bottom panel (strong synapses): The excitatory synapses are $g_{SI} = 30$ nS. The inhibitory synapses are $g_{IS} = 15$ nS. The lag between the peak of the EPSG and the action potential of I-cell is 6 ms. The histograms on the right show the distribution of spike time differences across the experiment. Note that the cells are not exactly antiphase due to differences in the cells involved. This is reflected in the fact that the upper trace of the bottom panel, giving the phase lag from cell 1 to cell 2, is not exactly the same as the lower trace of the bottom panel, giving lag from cell 2 to cell 1. Though both excitatory and inhibitory conductances were changed, the later modeling revealed that it is primarily the excitatory conductance change that accounted for the results.

previous section). Consider the function $\psi_{IS}(\Delta)$ computed from equation 3.5 for $\delta = 0$ and $\delta = 20$ (see Figure 10). The antiphase equilibrium points cor-respond to intercepts of $\psi_{IS}(\Delta)$ with the main diagonal. For both $\delta = 0$ and $\delta = 20$, the antiphase solutions are stable because the slope at the intercept is between -1 and 1, and hence the slope of the full map $\psi_{IS}^2(\Delta)$ is also between -1 and 1.

The noise in the S-cells can be interpreted geometrically as adding a random term to the value of $\psi_{IS}(\Delta)$ (which can be negative or positive) on each iteration of the map. In Figure 10 we show five such iterations for
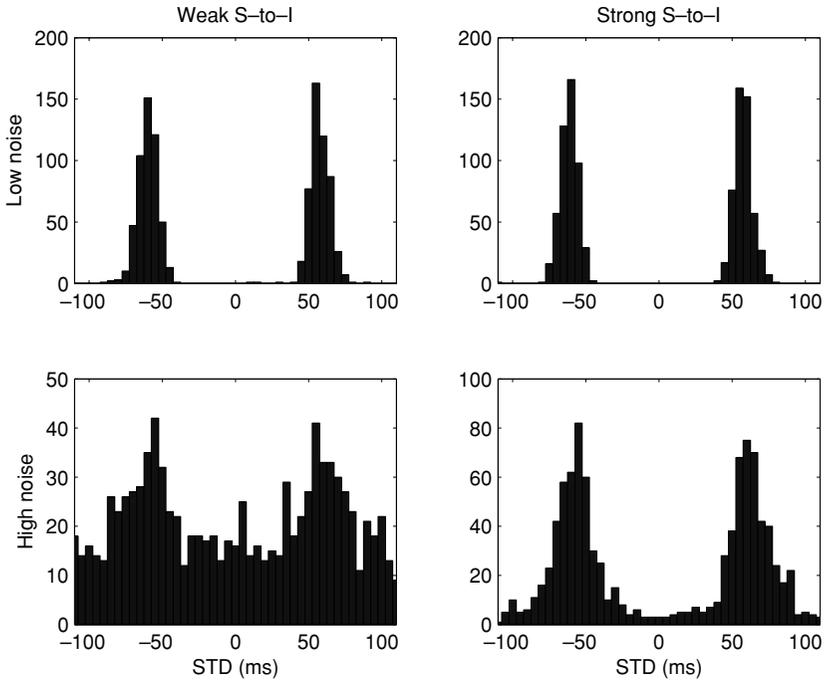
Figure 9: Distribution of spike time differences (STD) between S-cells in S-I-S network with weak ($g_{SI} = 0.01$) and strong S-to-I synapses ($g_{SI} = 0.05$) at two levels of noise: high ($N_{max} = 500$) and low ($N_{max} = 5000$). The S-cells were biased to fire on average with 120 ms interval.

$\delta = 0$ and $\delta = 20$, starting at the same initial conditions and applying the same sequence of random perturbations to both. For $\delta = 0$, the trajectory remains in the vicinity of the antiphase fixed point, while for $\delta = 20$ it goes much further; that is, an identical sequence of perturbations can cause more spread distribution of phases when S-to-I synapses are weak than when they are strong. This explains why the predicted antiphase behavior in the dynamic clamp experiment was observed only at larger values of S-I synaptic conductance.

3.2.5 Inhibition and h-Current. The difference in network behavior between $\tau = 20$ and $\tau = 5$ shows up only when the conductance of the h-current is very small or zero. When the h-conductance in the O-O network is reduced, the antiphase fixed point remains stable, while the in-phase fixed point changes from unstable to stable (see Figure 3C). Thus, in the O-O network, both in-phase and antiphase fixed points are stable when the h-conductance is reduced. Note the appearance of two other fixed
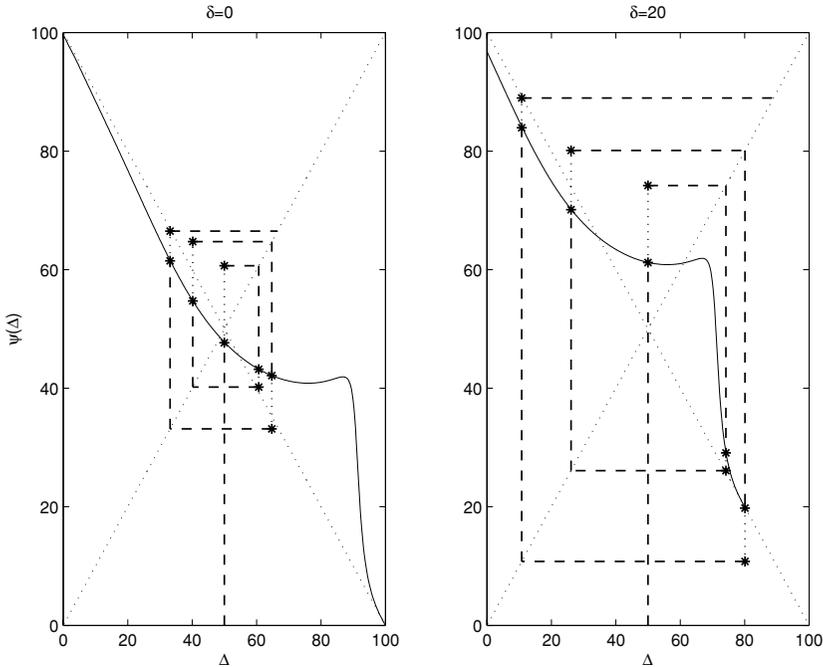
Figure 10: The map $\psi_{IS}(\Delta)$ defined by equation 3.5. The values of δ are 0 ms (left panel) and 20 ms (right panel). The dashed line represents a trajectory of the iterated map. The initial conditions are $t_0 = 50$ ms for both values of δ. The sequence of perturbations (dotted segments between asterisks) is 13 ms, −3 ms, 10 ms, −9 ms, and 5 ms for both values of δ.

points—neither in-phase nor antiphase (see Figure 3C, dotted line); they are both unstable as predicted by the slopes at the fixed points. In the S-I-S network, a decrease in the h-conductance does not change the stability of either fixed point; the in-phase remains stable, and the antiphase remains unstable (see Figure 4C).

In Figure 11 we focus on the transition of the h-current conductance from small to infinitesimal level ($g_h \simeq 0$). In the S-I-S network, the in-phase solution changes from unstable (g_h small) to stable ($g_h \simeq 0$), while the antiphase remains stable. Since for $g_h \simeq 0$ they are both stable, two other unstable fixed points appear as above. In the O-O network, the antiphase fixed point changes from stable (g_h small) to unstable ($g_h \simeq 0$). Note that the STDM for $g_h \simeq 0$ is not defined at the ends of the period due to violation of equation 3.1. Although in this case we cannot rigorously predict synchrony, we expect the in-phase to be stable as points everywhere else in the
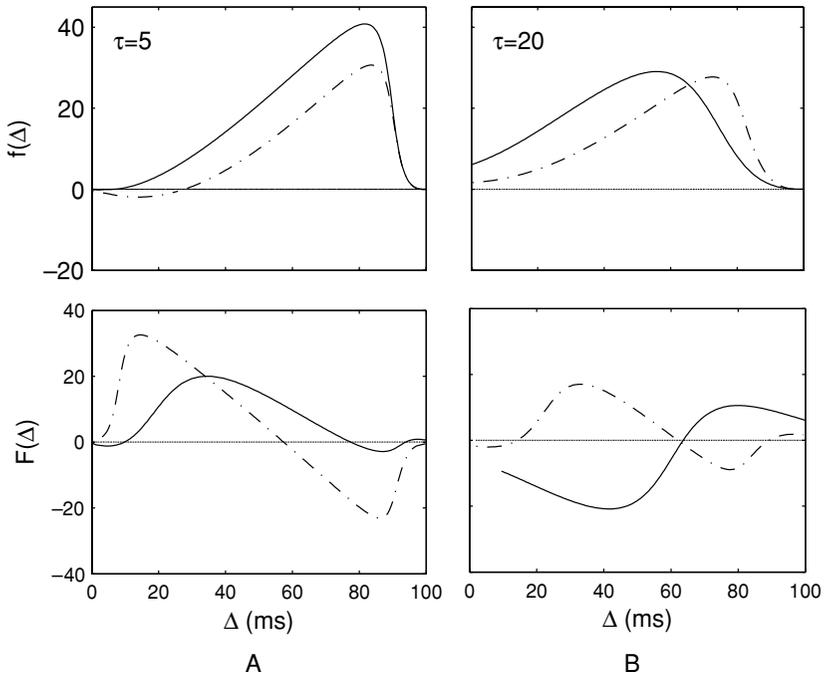
Figure 11: The transition of the h-current conductance from small to infinitesimal level in the S-I-S network (A) and the O-O network (B). (Top panels) STRCs for $g_h = 0.1$ (dot-dashed) and $g_h = 0$ (solid). (Bottom panels) The corresponding STDMs (same line types). The values of the compensatory DC current are $I_{app} = 0.895$ for $g_h = 0.1$ and $I_{app} = 1.314$ for $g_h = 0.0$. The other parameters are $g_{IS} = 0.04$, $g_{SI} = 0.10$, and $g_{OO} = 0.01$.

period go away from one another. All these observations are summarized as follows:

	$\tau = 20$		$\tau = 5$	
	In-phase	Antiphase	In-phase	Antiphase
Large Ih	Unstable	Stable	Unstable	Stable
Low Ih	Stable	Stable	Unstable	Stable
$g_h \simeq 0$	Stable	Unstable	Stable	Stable

The domain of stability for the antiphase solution is the region between the pair of fixed points surrounding the antiphase fixed point; for the in-phase solution, it is the union of regions surrounding $\Delta = 0$ and $\Delta = T$. In

each of these cases, the domains can be read off from Figures 3C, 4C, and 11A. This formulation does not work for Figure 11B, where the domains of stability cannot be correctly defined (see section 4). For young animals, the real neurons are most likely to operate with I_h lower than in adults (Richter, Klee, Heinemann, & Eder, 1997); one may expect $g_h \simeq 0$ in animals with I_h knocked out.

3.3 O-I-O Network. In the previous section, we reduced a three-cell model to a two-cell model by showing that the I-cell inhibition could be replaced by inhibition to the other S-cell produced by each S-cell, along with self-inhibition. In this section, we reduce a three-cell network that consists of two O-LM cells and one FS cell (see Figure 1C) to a per-turbation of a two-cell network that consists of one O-LM and one FS cell.

We start with those two cells, the O-cell producing IPSPs in the I-cell with a decay time of $\tau = 20$ ms and the I-cell producing an IPSP in the O-cell with a decay time of $\tau = 5$ ms (synapse rise time is un-changed). As explained in section 2, each of these pulses is associated with a STRC. Using the previous notation, these STRCs are denoted by $f_{OI}(\Delta)$ and $f_{IO}(\Delta)$. Since the O-cell has the same currents and parameters as the S-cell, $f_{IO}(\Delta)$ is the same as $f_{IS}(\Delta)$, which was previously shown in Figure 4A. The function $f_{OI}(\Delta)$ is plotted in Figure 12A; it is very simi-lar to $f_{OO}(\Delta)$ when $g_h = 0$ because the model of O-cell without h-current differs from the model of I-cell only by the presence of persistent sodium current.

We first use these STRCs to show that there is a stable fixed point for the O-I network. Assume that the O-cell spikes first, and let θ de-note the time difference until the spike of the I-cell. From the STRCs, we can compute the function $\psi_{OI}(\theta) = T_I + f_{OI}(\theta) - \theta$, and similarly for $\psi_{IO}(\theta) = T_O + f_{IO}(\theta) - \theta$, with the indices O and I reversed. These play the same role as ψ_{IS} in the S-I-S network (see equation 3.4) in producing the STDM, the map that takes θ to the time differ-ence in the next cycle, which we call $\bar{\theta}$. We write this map in the form

$$\bar{\theta} = \theta + F_{OI}(\theta) = \psi_{OI}(\psi_{IO}(\theta)). \tag{3.9}$$

Here F_{OI} plays the same role as F_{OO} and F_{SS} of the previous sections. As before, the right-hand side is a composition of two maps. In this case, however, the maps are not the same, reflecting the lack of symmetry in the network. The function F_{OI} is plotted in Figure 12B for several values of g_h. Recall that a zero of the map F is a fixed point of the map (see equation 3.9). For each value of g_h, there is a stable antiphase fixed point; the in-phase fixed point is also stable, but its domain of attraction is tiny.
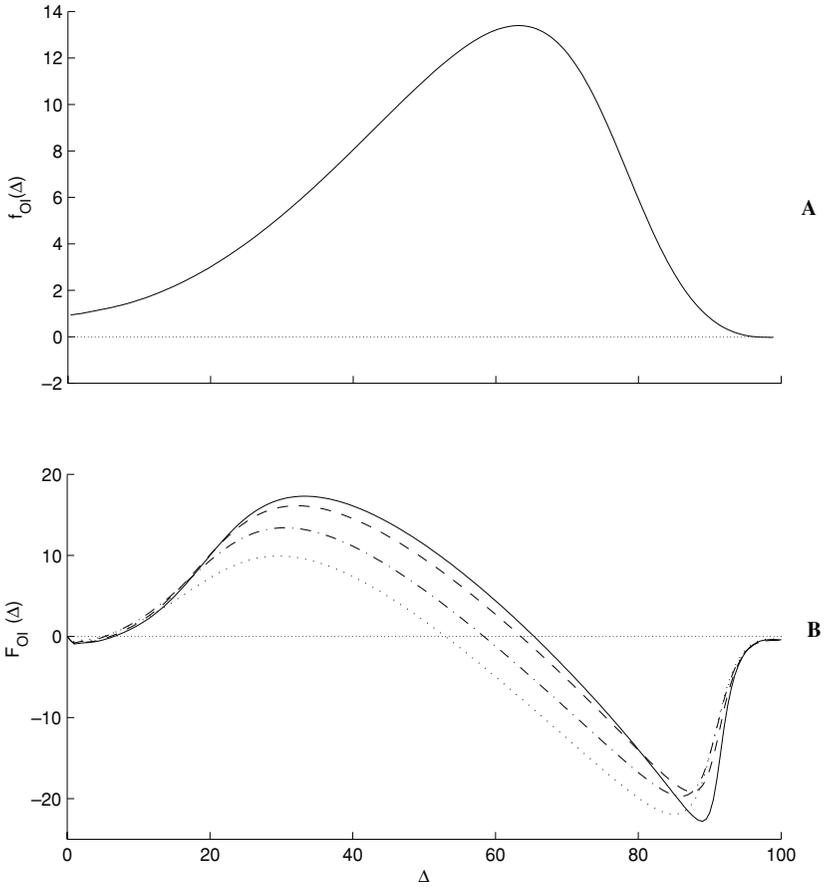
Figure 12: (A) The STRC $f_{OI}(\Delta)$. The conductance of O-to-I synapse is 0.02. (B) The STDMs for the O-I network. The values of g_h are 1.5, 1.0, 0.5, and 0.3 (solid, dashed, dot-dashed, and dotted, respectively). The compensatory DC currents are the same as in Figure 3; $g_{OI} = 0.02$.

We now show that the entire O-I-O network can be considered as a perturbation of an O-I network in which value g_{OI} is doubled. The latter network corresponds to the O-I-O network in which the two O-cells are synchronous, and hence the effect of the simultaneous inhibition on the I-cell is twice that of a single cell. Let t_1, t_2, and t_3 be the spike times of O_1, O_2, and I, respectively, and let $\bar{t}_1$, $\bar{t}_2$, and $\bar{t}_3$ be their spike times on the next cycle. We assume that the cells spike in this order: $\Delta = t_2 - t_1 > 0$ and $\theta = t_3 - t_2 > 0$. We have $\bar{t}_1 = t_1 + T_O + f_{IO}(\Delta + \theta)$ and $\bar{t}_2 = t_2 + T_O + f_{IO}(\theta)$. Then
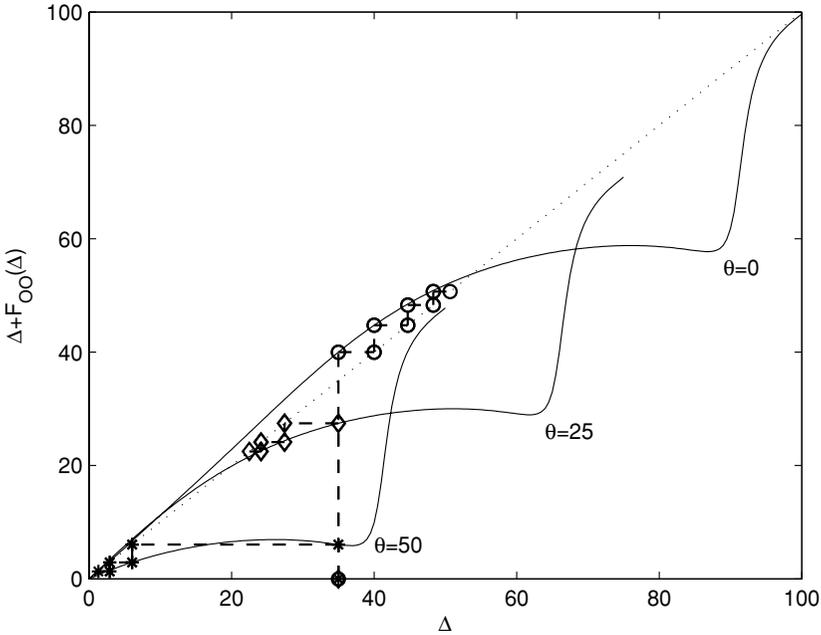
Figure 13: The map $\bar{\Delta} = \bar{\Delta}(\Delta)$ defined by equation 3.10. Three solid curves correspond to $\theta = 50$ ms, $\theta = 25$ ms, and $\theta = 0$ ms, as marked in the figure. The dashed lines represent trajectories of the iterated map, which starts at $\Delta = 35$ ms. Asterisks, diamonds, and circles denote iterations of $\bar{\Delta}$ for $\theta = 50$ ms, $\theta = 25$ ms, and $\theta = 0$ ms, respectively.

$\bar{\Delta} = \bar{t}_2 - \bar{t}_1 = \Delta + f_{IO}(\theta) - f_{IO}(\Delta + \theta)$. For fixed value of theta, consider the map

$$\bar{\Delta} = \Delta + f_{IO}(\theta) - f_{IO}(\Delta + \theta) = \Delta + F_{OO}(\Delta). \tag{3.10}$$

The function $\bar{\Delta}$ is shown in Figure 13. Note that if θ is large enough ($\theta = 50$), then the three-cell network approaches a regime in which the two O-cells are synchronous after one or two cycles; this happens for a relatively large range of initial values of Δ. Even after first interation, the two O-cells are close enough to be considered as one "composite" cell, with inhibition onto the I-cell twice as strong as one of a single cell. After Δ becomes close to zero, θ achieves its equilibrium according to equation 3.9. For smaller values of θ, Δ does not converge to zero. Thus, it is important that θ is large enough, that is, if the I-cell does not spike shortly after one of the O-cells. The latter condition holds when the O-to-I synaptic conductance is large enough and synapse decay time is long ($\tau = 20$). With weak O-to-I synapses

or fast decay of the inhibition, the synchrony in the O-I-O network becomes unstable.

4 Discussion

The methods used here are closely related to those of phase response curves (Winfree, 1980), long used to understand how periodic input to an oscillator can entrain the latter. In more recent work, those methods have been used to investigate the circumstances in which a pair of coupled oscillators interacting via pulses can synchronize or not (Goel & Ermentrout, 2002; Oprisan, Prinz, & Canavier, 2004; Gutkin, Ermentrout, & Reyes, 2005; Acker et al., 2003; Kopell & Ermentrout, 2002). The methodological novelty of the analysis in this article is the use of such methods for more than two cells. In two distinct ways, a three-cell network was shown to behave like a related two-cell network. For the network of two stellates and a FS cell, the latter was shown to behave, in some parameter regimes, as if the stellates were coupled directly by fast-decaying inhibition. The added FS cell acted to make the S-cells go in antiphase. When an FS interneuron was added to a network of O-LM cells, the network behaved (again, in some parameter regimes) like one with a single O-LM cell, with twice the coupling to the I-cell; the added FS cell synchronized the O-LM cells, which do not synchronize in the absence of that kind of cell. The central difference between the two situations is that the stellate cells excite the FS cell, while the O-LM cells inhibit the FS cell. Different methods of analysis were needed for the two cases. We note that the analysis we did with the three-cell networks cannot be done with weak coupling, since the synchrony described depends on the coupling being strong enough. Also, in Netoff, Acker, Bettencourt, and White (2005), it was shown experimentally that physiologically relevant inputs give rise to outputs that violate weak coupling assumptions (see also Preyer & Butera, 2005, for synapses in an invertebrate preparation).

The STRCs obtained in the dynamic clamp experiment are in good agreement with analytical STRCs (see Figures 3 and 4). The inhibitory stimuli that arrive in the beginning of the period cause advance of the next spike; for S-cells this advance is more substantial than for O-LM cells and increases with increasing g_h. In the middle of the period, inhibition delays the next spike for both O-LM and S-cells. The most significant distinction between analytical and experimental STRCs is observed for the S-cells at the end of the period, where the model neuron is affected by the inhibition much less than the in vitro neuron. This leads to an underestimation in the analysis of the domain of stability of the in-phase solution in the S-I-S network.

The reduced two-cell analysis of the S-I-S network can be extended to account for the behavior when there is a significant delay between the firing of an S-cell and that of the I-cell. This occurs when the excitation from an S-cell to an I-cell is sufficiently weak (Ermentrout & Kopell, 1998). Analysis showed that such a delay does not change the antiphase behavior of the

S-cells in a deterministic case, but in cooperation with noise inherently present in I-to-S synapses, it results in great variability of phases between S-cells.

A two-cell reduction is also possible for larger networks with all-to-all connections consisting of more than one I-cell and more than two S-cells. In such a network, there is another source of variability—one that comes from the initial conditions and results in formation of synchronous cell assemblies (clusters) in both S- and I-cells populations. In the situation relevant to the theta rhythm (approximately 10 Hz), there are two such cell ensembles for the S-cell population and one ensemble for the I-cell population, which behave as aggregate units very similarly to the S-cells and the I-cell in the three-cell network. Depending on the initial conditions, these units may contain different number of cells; this leads to nonequivalent synapses and, as a consequence, to lack of the symmetry in that network.

The difference in network behavior caused by delays is explained by Figure 9 only if assumptions 1 to 5 are valid. Direct simulations show that the I-cell sometimes skips a cycle as a result of overlap of phasic EPSPs from the S-cells when S-to-I synapses are weak. This violates assumption 2 and results in a pattern of firing that is different from one stated in the assumption 3; the latter was necessary for construction of the map (see equation 3.4). Also, assumption 4 is violated when δ is large. In this situation, another force plays a more dominant role: both S-cells receive common inhibition, which is known to facilitate synchrony in other excitatory cells (Terman et al., 1998; Börgers & Kopell, 2003). This common inhibition can help to explain several synchronous spikes, which appeared in Figure 8 even with strong S-to-I synapses.

The fact that our STDMs are not applicable to the analysis of synchrony in the O-O network (see Figure 11) has to do with the usual assumption of the STRC method that each stimulus influences only the next spike, not the subsequent ones. This is not the case in the O-O network. According to Figure 11, the spike of O_1 that arrives a few milliseconds before the spike of O_2 has very little effect on the timing of the latter; however, the next spike of O_2 is delayed (even in absence of O_1 activity) because the inhibition lasts long and affects O_2 after its first spike. In other words, the inhibition with $\tau = 5$ ms can be considered as an instant pulse, while one with $\tau = 20$ ms cannot. In the presence of O_1 activity, this would cause a switch of leadership between O_1 and O_2. The technique of spike time responses can be adopted to this case by defining the second-order STRC as in Oprisan et al. (2004).

The analysis of the stellate/FS network was motivated by data of Cunningham and Whittington (Cunningham, Pervouchine, Kopell, & Whittington, 2004) in slices of medial entorhinal cortex. If the activation from kainate is sufficiently low, the slice displays slow (< 1 Hz) oscillations in the electrical activity of the stellate cells, alternating between a silent regime and an active one. Within the latter, the spectrum of the activity contains peaks at both beta (centered around 21 Hz) and theta (centered around

9 Hz) frequencies. Since the main cells involved in the active regime are the stellates and the FS interneurons, the origin of the beta peak is mysterious. The work presented here suggests a possible solution: since the stellate cells are in antiphase, the population frequency is twice as fast, producing a beta frequency. In larger network simulations, with many stellates and FS cells, the stellates break into two clusters, each firing at a theta rhythm, with a population rhythm twice as fast (data not shown); as long as the clusters are not of the same size (the generic case), there is also a theta peak in the spectrum.

The STRC/STDM technique goes beyond the information acquired about these particular models and shows how to do such an analysis when the model is changed. For example, other models of the stellate cell (Acker et al., 2003; Alonso & Klink, 1993) contain an M-current instead of, or in addition to, the h-current. A similar analysis can show how changes in the biophysics of the intrinsic or synaptic models can change the network outcome. The STRCs contain the information needed about the biophysics to make predictions about network behavior. However, the transition from STRCs to the maps that predict network dynamics depends on assumptions about the order in which spikes occur in the different cells. Thus, a single map cannot necessarily embody all the possible dynamical behaviors of the network; each map is valid in some (possibly very large) set of trajectories but can fail when the spike order changes. Such a bifurcation cannot be investigated within that map but requires consideration of the full system.

Appendix

A.1 Dynamic Models of Neurons. Voltage-dependent conductances are modeled using a Hodgkin-Huxley type of kinetic model. The cells in the network are indexed with a symbol $i \in \Omega$. The current-balance equation for all types of cells is

$$C_i \frac{\partial v_i}{\partial t} = I_{app,i} - \sum I_{ion,i} - \sum_{j \in \Omega} I_{syn,j \to i},$$

where v_i and C_i are the membrane potential (mV) and membrane capacitance ($\mu F/cm^2$) of the ith cell, $I_{app,i}$ is the bias (DC) current (μA) applied to the ith cell, and $I_{ion,i}$ and $I_{syn,j \to i}$ are the respective sums of ionic and synaptic currents. The sum of ionic currents is

$$\sum I_{ion,i} = I_{Na,i} + I_{K,i} + I_{L,i} + I_{Nap,i} + I_{h,i},$$

for the O- and S-cells and

$$\sum I_{ion,i} = I_{Na,i} + I_{K,i} + I_{L,i}$$

for the I-cells, where

$$I_{Na,i} = g_{Na,i} m_i^3 h_i (v_i - E_{Na,i}),$$

$$I_{K,i} = g_{K,i} n_i^4 (v_i - E_{K,i}),$$

$$I_{L,i} = g_{L,i} (v_i - E_{L,i}),$$

$$I_{Nap,i} = g_{Nap,i} p_i (v_i - E_{Na,i}),$$

$$I_{h,i} = g_{h,i} (0.65 h_i^f + 0.35 h_i^s)(v_i - E_{h,i}).$$

In the expressions for ionic currents, $g_{X,i}$ are the maximal conductances (mS/cm^2) and $E_{X,i}$ are the reversal potentials (mV), and m_i, h_i, n_i, p_i, h_i^f, and h_i^s are the respective channel gating variables (see below). Units of time are ms. The following maximal conductances and reversal potentials are used for the O- and S-cells: $E_{Na,i} = 55$, $E_{K,i} = -90$, $E_{L,i} = -65$, $E_{h,i} = -20$, $g_{Na,i} = 52$, $g_{K,i} = 11$, $g_{L,i} = 0.5$, $g_{Nap,i} = 0.5$, $g_{h,i} = 1.5$, and $C_i = 1.5$. For the I-cells, the following maximal conductances and reversal potentials are used: $E_{Na,i} = 50$, $E_{K,i} = -100$, $E_{L,i} = -67$, $g_{Na,i} = 100$, $g_{K,i} = 80$, $g_{L,i} = 0.1$, and $C_i = 1.5$. The gating variables $x_i = m_i$, h_i, n_i, p_i, h_i^f, and h_i^s obey a first-order differential equation of the following form:

$$\frac{\partial x_i}{\partial t} = (x_{i,\infty}(v_i) - x_i) / \tau_{x,i}(v_i),$$

where

$$x_{i,\infty}(v) = \frac{\alpha_{x,i}(v)}{\alpha_{x,i}(v) + \beta_{x,i}(v)}$$

$$\tau_{x,i}(v) = \frac{1}{\alpha_{x,i}(v) + \beta_{x,i}(v)}.$$

Here $\alpha_{x,i}(v)$ and $\beta_{x,i}(v)$ are the corresponding channel's opening and closing rates. For O- and S-cells, the following channel opening and closing rates are used:

$$\alpha_{m,i}(v) = -0.1 (v + 23) / (e^{-0.1(v+23)} - 1)$$

$$\beta_{m,i}(v) = 4 e^{-(v+48)/18}$$

$$\alpha_{h,i}(v) = 0.07 e^{-(v+37)/20}$$

$$\beta_{h,i}(v) = 1 / (e^{-0.1(v+7)} + 1)$$

$$\alpha_{n,i}(v) = -0.01 (v + 27) / (e^{-0.1(v+27)} - 1)$$

$$\beta_{n,i}(v) = 0.125 e^{-(v+37)/80}$$

$$\alpha_{p,i}(v) = 1 / (0.15 (1 + e^{-(v+38)/6.5}))$$

$$\beta_{p,i}(v) = e^{-(v+38)/6.5} / (0.15 (1 + e^{-(v+38)/6.5}))$$

$$h_{i,\infty}^f(v) = 1 / (1 + e^{(v+79.2)/9.78})$$

$$\tau_{h^f,i}(v) = 0.51 / (e^{(v-1.7)/10} + e^{-(v+340)/52}) + 1$$

$$h_{i,\infty}^s(v) = 1 / (1 + e^{(v+2.83)/15.9})^{58}$$

$$\tau_{h^s,i}(v) = 5.6 / (e^{(v-1.7)/14} + e^{-(v+260)/43}) + 1.$$

The channel opening and closing rates for the I-cells are:

$$\alpha_{m,i}(v) = 0.32 (54 + v) / (1 - e^{-(v+54)/4})$$

$$\beta_{m,i}(v) = 0.28 (v + 27) / (e^{(v+27)/5} - 1)$$

$$\alpha_{h,i}(v) = 0.128 e^{-(50+v)/18}$$

$$\beta_{h,i}(v) = 4 / (1 + e^{-(v+27)/5})$$

$$\alpha_{n,i}(v) = 0.032 (v + 52) / (1 - e^{-(v+52)/5})$$

$$\beta_{n,i}(v) = 0.5 e^{-(57+v)/40}.$$

A.2 Synapses. The synaptic currents for all types of cells has the following form:

$$I_{syn,j \to i} = \tilde{g}_{ji} s_j (v_i - E_{rev,j}),$$

where $\tilde{g}_{ji}$, s_j, and $E_{rev,j}$ are the maximal conductance of $j \to i$ synapse, the synaptic gating variable of the jth cell, and the synaptic reversal potential of the jth cell, respectively. The reversal potentials of I-, O-, and S-cells are -70 mV, -70 mV, and 0 mV, respectively. The value of the maximal synaptic conductance is normalized to the area under IPSP (or EPSP) such that $\tilde{g}_{ji} = g_{ji}/\tau_{ji}$, where τ_{ji} is the decay time of $j \to i$ synapse, and g_{ji} is the value of maximal synaptic conductance reported in the text.

A.3 Stochastic Simulations. In the stochastic simulations, the term $g_{Nap,i} \cdot p_i$ in the equation for the persistent sodium current ($I_{Nap,i}$) is replaced by the stochastic term $\gamma N_i / SA$ as in previous works (White, Klink, Alonso, & Kay, 1998; Acker et al., 2003). Here N_i is the number of open persistent sodium channels and varies from 0 to N_{max}, $\gamma = 20$ pS is the open channel conductance, and $SA = 2.29 \cdot 10^{-4}$ cm^2 is the cell's surface area. The values of γ, N_{max}, and SA are such that the maximal conductance is equal to $g_{Nap,i}$ in the deterministic model. The channels are assumed to be independent and identical. On each step of the simulation, a random
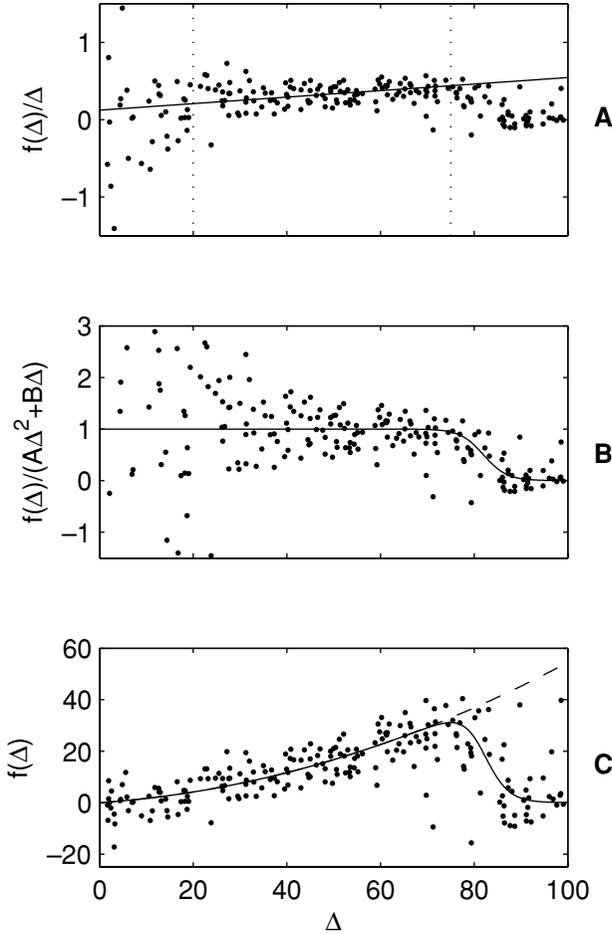
Figure 14: Curve fitting (the data from Figure 3 are used). (A) Linear regression, $A \cdot \Delta + B$, of $f(\Delta)/\Delta$ versus Δ; the range of Δ is between dotted vertical lines. (B) Multiplicative residuals $f(\Delta)/(A \cdot \Delta^2 + B \cdot \Delta)$ are fit with the function $\tanh((C - \Delta)/D)$ using nonlinear least-square optimization (border constraints: $50 \leq C \leq 90$, $0.01 \leq D \leq 100$). (C) The resulting fit is $f(\Delta) \simeq (A \cdot \Delta^2 + B \cdot \Delta)\tanh((C - \Delta)/D)$ (solid); compare to the quadratic fit (dashed).

number is chosen from an exponential distribution based on the equations $\alpha_{p,i}(V)$ and $\beta_{p,i}(V)$ above to determine the time of the next channel transition. The equations are then integrated up to that time, and the number of open channels is updated. This method is generally used for exact stochastic simulations of chemical reactions (Gillespie, 1977).

A.4 Curve Fitting. Experimental data were fit using a nonlinear model as follows. First, we obtain a linear fit, $A \cdot \Delta + B$, for the function $f(\Delta)/\Delta$ versus Δ in a certain range of Δ (see Figure 14A). For $f(\Delta)$, this gives a quadratic fit, $A \cdot \Delta^2 + B \cdot \Delta$, which passes through the origin (see Figure 14B, dashed line). Then the multiplicative residuals $f(\Delta)/(A \cdot \Delta^2 + B \cdot \Delta)$ are fit with the function $\tanh((C - \Delta)/D)$, where $\tanh(x) = (e^x - e^{-x})/(e^x + e^{-x})$, using nonlinear least-square optimization (see Figure 14C). The resulting fit is $f(\Delta) \simeq (A \cdot \Delta^2 + B \cdot \Delta)\tanh((C - \Delta)/D)$ (see Figure 14B, solid line).

Acknowledgments

References

Acker, C. D., Kopell, N., & White, J. A. (2003). Synchronization of strongly coupled excitatory neurons: Relating network behavior to biophysics. *J. Comp. Neurosci., 15*(1), 71–90.

Adey, W. R., Dunlop, C. W., & Hendrix, C. E. (1960). Hippocampal slow waves: Distribution and phase relationship in the course of approach learning. *Arch. Neurol., 3*, 74–90.

Adey, W. R., Sunderland, M. D., & Dunlop, C. W. (1957). The entorhinal area: Electrophysiological studies of its interrelations with rhinencephalic structures and the brainstem. *Electroencephalography and Clinical Neurophysiology, 9*(3), 309–324.

Alonso, A., & García-Austt, E. (1987). Neuronal sources of theta rhythm in the entorhinal cortex of the rat. II. Phase relations between unit discharges and theta field potentials. *Exp. Brain Res., 67*(3), 502–509.

Alonso, A., & Klink, R. (1993). Differential electroresponsiveness of stellate and pyramidal-like cells of medial entorhinal cortex layer II. *J. Neurophysiol., 70*, 128–143.

Börgers, C., & Kopell, N. (2003). Synchronization in networks of excitatory and inhibitory neurons with sparse, random connectivity. *Neurocomp., 15*(3), 509–538.

Crook, S. M., Ermentrout, B., & Bower, J. M. (1998). Spike frequency adaptation affects the synchronization properties of networks of cortical oscillator. *Neural Computation, 4*, 837–854.

Cunningham, M. O., Davies, C. H., Buhl, E. H., Kopell, N., & Whittington, M. A. (2003). Gamma oscillations induced by kainate receptor activation in the entorhinal cortex in vitro. *Journal of Neuroscience, 23*(30), 9761–9769.

Cunningham, M. O., Pervouchine, D. D., Kopell, N., & Whittington, M. (2004). Cellular and network mechanisms of slow activity (<1 Hz) in the entorhinal cortex. *Society for Neuroscience Meeting 2004*, Abstract 638.9.

Destexhe, A., Mainen, Z. F., & Sejnowski, T. J. (1998). Kinetic models of synaptic transmission. In C. Koch & I Seger (Eds.), *Methods in neuronal modeling* (2nd Ed.). Cambridge, MA: MIT Press.

Dickson, C. T., Magistretti, J., Shalinsky, M. H., Fransén, E., Hasselmo, M. E., & Alonso, A. A. (2000). Properties and role of Ih in the pacing of subthreshold oscillations in entorhinal cortex layer II neurons. *J. Neurophysiol., 83*, 2562–2579.

Dickson, C. T., Magistretti, J., Shalinsky, M., Hamam, B., & Alonso, A. (2000). Oscillatory activity in entorhinal neurons and circuits: Mechanisms and function. *Ann. N.Y. Acad. Sci., 911*, 127–150.

Dorval, A. D., Christini, D. J., & White, J. A. (2001). Real-time Linux dynamic clamp: A fast and flexible way to construct virtual ion channels in living cells. *Annals of Biomedical Engineering, 29*, 897–907.

Ermentrout, G. B., & Kopell, N. (1998). Fine structure of neural spiking and synchronization in the presence of conduction delays. *Proc. Natl. Acad. Sci. USA, 95*, 1259–1264.

Ermentrout, B., Pascal, M., & Gutkin, B. S. (2001). The effects of spike frequency adaptation and negative feedback on the synchronization of neural oscillators. *Neural Computation, 13*, 1285–1310.

Gillespie, D. T. (1977). Exact stochastic simulation of coupled chemical reactions. *Journal of Physical Chemistry, 81*, 2340–2361.

Gillies, M. J., Traub, R. D., LeBeau, F. E. N., Davies, C. H., Gloveli, T., Buhl, E. H., & Whittington, M. A. (2002). A model of atropine-resistant theta oscillations in rat hippocampal area CA1. *Journal of Physiology, 543*(3), 779–793.

Goel, P., & Ermentrout, B. (2002). Synchrony, stability, and firing patterns in pulse-coupled oscillators. *Physica D, 163*, 191–216.

Gutkin, B. S., Ermentrout, G. B., & Reyes, A. D. (2005). Phase-response curves give the responses of neurons to transient inputs. *J. Neurophysiol., 94*, 1623–1635.

Hájos, N., & Mody, I. (1997). Synaptic communication among hippocampal interneurons: Properties of spontaneous IPSCs in morphologically identified cells. *J. Neurosci., 17*, 8427–8442.

Jones, R. S., & Buhl, E. H. (1993). Basket-like interneurones in layer II of the entorhinal cortex exhibit a powerful NMDA-mediated synaptic excitation. *Neurosci. Lett., 149*(1), 35–39.

Kopell, N., & Ermentrout, G. B. (2002). Mechanisms of phase-locking and frequency control in pairs of coupled neural oscillators. In B. Fiedler (Ed.), *Handbook on dynamical systems: Toward applications* (Vol. 2, pp. 3–54). Dordrecht: Elsevier.

Kopell, N., Ermentrout, G. B., Whittington, M., & Traub, R. D. (2000). Gamma rhythms and beta rhythms have different synchronization properties. *Proc. Nat. Acad. Sci. USA, 97*, 1867–1872.

Lacaille, J.-C., Williams, S., Kunkel, D., & Schwartzkroin, P. (1987). Local circuit interactions between oriens/alveus interneurons and CA1 pyramidal cells in hippocampal slices: Electrophysiology and morphology. *J. Neurosci., 7*, 1979–1993.

Lewis, T. J. (2003). Phase-locking in electrically coupled non-leaky integrate-and-fire neurons. *Discrete Contin. Dyn. Syst. Ser. B* (Suppl.), 554–562.

Maccaferri, G., & McBain, C. (1996). The hyperpolarization-activated current (I_h) and its contribution to pacemaker activity in rat CA1 hippocampal stratum oriens-alveus interneurones. *J. Physiol., 497*, 119–130.

Netoff, T. I., Acker, C. D., Bettencourt, J. C., & White, J. A. (2005). Beyond two-cell networks: Experimental measurement of neuronal responses to multiple synaptic inputs. *Journal of Computational Neuroscience, 18*, 287–295.

Netoff, T. I., Banks, M. I., Dorval, A. D., Acker, C. D., Haas, J. S., Kopell, N., & White, J. A. (2004). Synchronization in hybrid neuronal networks of the hippocampal formation. *J. Neurophysiol.*, doi:10.1152/jn.00982.2004.

Oprisan, S. A., Prinz, A. A., & Canavier, C. C. (2004). Phase resetting and phase locking in hybrid circuits of one model and one biological neuron. *Biophys. J., 87*, 2283–2298.

Press, W., Teukolsky, S., William, T. V., & Brian, P. F. (1992). *Numerical recipes in C* (2nd ed.). Cambridge: Cambridge University Press.

Preyer, A. J., & Butera, R. J. (2005). Neuronal oscillators in *Aplysia californica* that demonstrate weak coupling in vitro. *Phys. Rev. Lett., 95*(13), 138103.

Richter, H., Klee, R., Heinemann, U., & Eder, C. (1997). Developmental changes in inward rectifier currents in neurons of the rat entorhinal cortex. *Neurosci. Lett., 228*, 139–141.

Rotstein, H. G., Pervouchine, D. D., Gillies, M. J., Acker, C. D., White, J. A., Buhl, E. H., Whittington, M. A., & Kopell, N. (2005). Slow and fast inhibition and an h-current interact to create a theta rhythm in a model of CA1 interneuron network. *J. Neurophysiol., 94*, 1509–1518.

Saraga, F., Wu, C. P., Zhang, L., & Skinner, F. K. (2003). Active dendrites and spike propagation in multi-compartment models of oriens-lacunosum/moleculare hippocampal interneurons. *J. Physiol., 552*, 502–509.

Strogatz, S. H. (1994). *Nonlinear dynamics and chaos: With applications to physics, biology, chemistry, and engineering*. Cambridge, MA: Perseus Books.

Terman, D., Kopell, N., & Bose, A. (1998). Dynamics of two mutually coupled slow inhibitory neurons. *Physica D, 117*, 241–275.

Traub, R. D., Whittington, M. A., Colling, S. B., Buzsaki, G., & Jefferys, J. G. (1996). Analysis of gamma rhythms in the rat hippocampus in vitro and in vivo. *J. Physiol., 493*, 471–484.

White, J. A., Budde, T., & Kay, A. R. (1995). A bifurcation analysis of neural subthreshold oscillations. *Biophysical Journal, 69*, 1203–1217.

White, J. A., Klink, R., Alonso, A., & Kay, A. R. (1998). Noise from voltage-gated ion channels may influence neuronal dynamics in the entorhinal cortex. *J. Neurophysiol., 80*, 262–269.

Winfree, A. T. (1980). *Geometry of biological time*. Berlin: Springer.

Witter, M., & Wouterlood, F. (2002). *The parahippocampal region*. New York: Oxford University Press.